THE JOURNAL OF BIOLOGICAL CHEMISTRY VOL. 283, NO. 19, pp. 13070–13076, May 9, 2008

New Insights into the Mechanism of RNA Degradation by Ribonuclease II

IDENTIFICATION OF THE RESIDUE RESPONSIBLE FOR SETTING THE RNase II END PRODUCT[*] [S]

Received for publication, December 7, 2007, and in revised form, March 12, 2008 Published, JBC Papers in Press, March 12, 2008, DOI 10.1074/jbc.M709989200

Ana Barbas[‡], Rute G. Matos[‡], Mónica Amblar[‡1], Eduardo López-Viñas[§], Paulino Gomez-Puertas[§], and Cecília M. Arraiano[‡2]

From the [‡]Instituto de Tecnologia Química e Biológica/Universidade Nova de Lisboa, Apartado 127, 2781-901 Oeiras, Portugal and [§]Centro de Biologia Molecular "Severo Ochoa", Campus Universidad Autonoma de Madrid and CIBER-Obn, Physiopathology of Obesity and Nutrition (CB06/03/0026), Instituto de Salud Carlos III, Madrid 28049, Spain

RNase II is a key exoribonuclease involved in the maturation, turnover, and quality control of RNA. RNase II homologues are components of the exosome, a complex of exoribonucleases. The structure of RNase II unraveled crucial aspects of the mechanism of RNA degradation. Here we show that mutations in highly conserved residues at the active site affect the activity of the enzyme. Moreover, we have identified the residue that is responsible for setting the end product of RNase II. In addition, we present for the first time the models of two members of the RNase II family, RNase R from *Escherichia coli* and human Rrp44, also called Dis3. Our findings improve the present model for RNA degradation by the RNase II family of enzymes.

Escherichia coli RNase II is the prototype of the RNase II superfamily of exoribonucleases, whose homologues are present in all three domains of life (1–4). RNase II and its homologues can be environmentally (5, 6) and developmentally regulated (7), and other ribonucleases have been shown to be involved in their post-transcriptional control (8–10). Mutations in the *rnb* gene have been linked with abnormal chloroplast biogenesis (11), mitotic control, and cancer (12). RNase II is a ubiquitous enzyme that degrades single-stranded RNAs processively in the 3′- to 5′-direction, resulting in the generation of 5′-mononucleotides. Ten nucleotides is the minimum length of the RNA molecule needed to detect activity in RNase II, and the end product of degradation of this enzyme is a 4-nucleotide RNA oligomer (13–15). RNase II homologues Dis3/Rrp44 are components of the exosome, a complex of exoribonucleases involved in the maturation and turnover of RNA (2), in RNA interference (16), and in surveillance pathways that recognize and degrade aberrant RNAs (17, 18). Recent reports have shown that Dis3/Rrp44 is the only catalytically active nuclease in the yeast core exosome (19) and plays a direct role in RNA surveillance, contributing to the recognition and degradation of specific RNA targets (20). In addition, the human exosome has hydrolytic activity, similar to what happens in the yeast exosome (13, 18, 21).[3] The RNase II homologues present in the exosome have the same behavior regarding the minimum length of RNA substrate and the same final end product as the *E. coli* RNase II (13, 18, 21). Moreover, the recent determination of the electron microscopy structure of yeast Rrp44 (22) showed that *E. coli* RNase II is a good model and suggests that the RNA recruitment mechanism is conserved.

The three-dimensional structure of *E. coli* RNase II was recently determined (23–25). The structure of RNase II RNA-bound complex (23, 24), together with biochemical data, gave new insights into the mechanisms of catalysis, translocation, and processivity of this important RNA-degrading enzyme. The *E. coli* RNase II structure and its RNA-bound complex have been used as a model for the analysis of Dis3/Rrp44 (20). RNase II consists of four domains (Fig. 1*A*): two N-terminal cold shock domains (CSD1 and CSD2), one central RNB catalytic domain, and one C-terminal S1 domain. The RNA contacts the enzyme at two different and non-contiguous regions, the anchoring and the catalytic regions, which act synergistically to provide a processive degradation. Nucleotides 1 to 5 are located in the anchor region, situated in a deep cleft between the two cold shock domains and the S1 domain (Fig. 1*A*). The catalytic region forms a cavity that is only accessible to single-stranded RNA, where the last five nucleotides at the 3′-end of the RNA molecule (nt 9–13) are stacked and clamped between the aromatic residues Tyr-253 and Phe-358. In a recent report (23) we postulated a model for RNA degradation that involves one Mg^{2+} ion, four highly conserved aspartic acids (201, 207, 209, and 210), and the recruitment of a second Mg^{2+} for catalysis. In this study we mutated these highly conserved amino acids present in the active site and characterized the respective proteins. Here, we also show, for the first time, the models of two related members of the RNase II family, RNase R from *E. coli* and human Rrp44 (Fig. 1, *B* and *C*). These results shed new light on the mechanism of RNA degradation by RNase II

* The work at the CBMSO was supported by "Ministerio de Educación y Ciencia" Grant SAF2004-06843 and by an institutional grant from "Fundación Ramón Areces." The work at the ITQB was supported by Fundação para a Ciência e a Tecnologia (FCT), Portugal. The costs of publication of this article were defrayed in part by the payment of page charges. This article must therefore be hereby marked "*advertisement*" in accordance with 18 U.S.C. Section 1734 solely to indicate this fact.

[S] The on-line version of this article (available at http://www.jbc.org) contains supplemental experimental procedures, supplemental references, and supplemental Figs. S1–S6.

[1] Present address: Centro de Investigaciones Biológicas, C/Ramiro de Maeztu, 9, 28040 Madrid, Spain.

[2] To whom correspondence should be addressed. Tel.: 351-214469547; Fax: 351-214411277; E-mail: cecilia@itqb.unl.pt.

[3] C. D. Lima, personal communication.

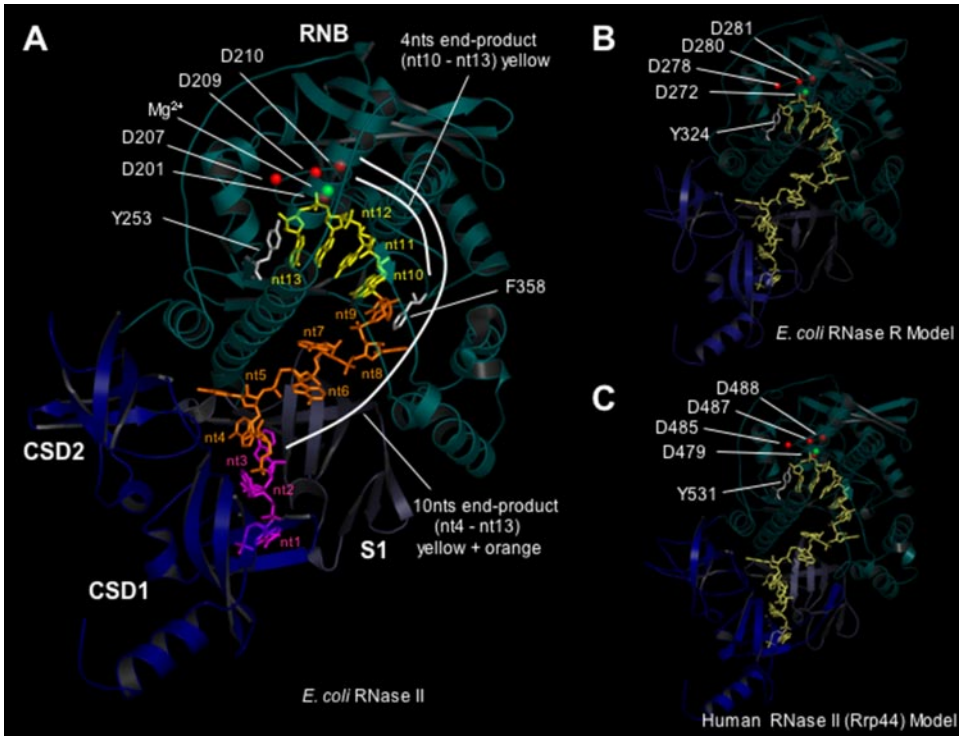

FIGURE 1. **Structure of *E. coli* RNase II-RNA complex and homology-based three-dimensional models of *E. coli* RNase R and human RNase II (*Rrp44*).** *A*, RNase II structure bound to a 13-nt RNA molecule (crystal 2ix1) indicating possible RNA degradation end products (4 nt, *yellow*, and 10 nt, *yellow plus orange*). Highly conserved residues mutated are indicated. The 5 nt at the 3′-end of the RNA molecule (nt 9–13) are stacked and clamped between the aromatic residues Tyr-253 and Phe-358. *B* and *C*, three-dimensional models of *E. coli* RNase R (amino acids 84–724) and human Rrp44 (amino acids 301–927) proteins, respectively, based on crystal structure 2ix1. Positions of all equivalent residues of the catalytic site of RNase II enzyme that were mutated in this report are indicated in all three proteins. Tyr-324 (*RNase R*) and Tyr-531 (*Rrp44*) are equivalent to RNase II Tyr-253 stacking residue. The human Rrp44 model does not include large insertions spanning residues Asp-166-Ser-254 and Ser-307-Arg-344 due to the lack of an appropriately aligned template structure.

and can therefore be important for comprehension of the mode of action of other members of the RNase II family.

EXPERIMENTAL PROCEDURES

Construction of RNase II Mutants by Site-directed Mutagenesis—Mutations D207N, D210N, F358A, and Y253A,F358A were introduced into pFCT6.9 (5) by PCR overlapping (26). D201N and Y253A mutations were generated by site-directed mutagenesis using QuikChange Site-directed Mutagenesis kit from Stratagene. The primers used in this study are described in supplemental experimental procedures.

Overexpression and Purification of Wild-type and RNase II Mutants—The plasmid used for expression of wild-type *E. coli* histidine-tagged RNase II protein was pFCT6.9 plasmid (5). All other plasmids bearing mutations were transformed into BL21(DE3) *E. coli* strain (Novagen) to allow the expression of the recombinant proteins. Purification of all proteins was performed by histidine affinity chromatography using HiTrap Chelating HP columns (GE Healthcare) and the AKTA HLPC system (GE Healthcare) following the protocol previously described (13). The purity of the enzymes was analyzed in an 8% SDS-PAGE (supplemental Fig. S1).

Activity Assays—Exoribonucleolytic activity was assayed using oligoribonucleotides as substrate (13). The 30-mer oligoribonucleotide (5′-CCCGACACCAACCACUAAAAAAA-AAAAAAA-3′) and the poly(A) chain of 35 nt were labeled at the 5′-end with [γ-^{32}P] ATP and T4 polynucleotide kinase. The RNA oligomers were then purified using Microcon YM-3 Centrifugal Filter Devices (Millipore). Reactions were carried out in a final volume of 10 μl containing 30 nM substrate, 20 mM Tris-HCl, pH 8, 100 mM KCl, 1 mM $MgCl_2$, and 1 mM dithiothreitol. The amount of each enzyme added to the reaction was adjusted to obtain linear conditions and is indicated in Fig. 2. Reactions were started by the addition of the enzyme and incubated at 37 °C. Samples were withdrawn at the time points indicated in the figure, and the reaction was stopped by adding formamide-containing dye supplemented with 10 mM EDTA. Reaction products were resolved in 20% polyacrylamide/7 M urea and analyzed by autoradiography. The exoribonucleolytic activity of the enzymes was determined by measuring and quantifying the disappearance of the substrate in three distinct experiments; each value obtained represents the mean of these independent assays (supplemental Fig. S2). The exoribonucleolytic activity of the wild-type enzyme was taken as 100%.

Surface Plasmon Resonance Analysis, Biacore—Biacore SA streptavidin chips were obtained from Biacore Inc. (GE Healthcare). The flow cells of the SA streptavidin sensor chip were coated with a low concentration of the substrates as described in supplemental experimental procedures. The biosensor assay was run at 4 °C in a buffer containing 20 mM Tris-HCl, pH 8, 100 mM KCl, 1 mM dithiothreitol, and 25 mM EDTA. The target RNA substrate was captured on flow cell 2, and the pure proteins were injected as indicated in supplemental experimental procedures. All experiments included triple injections of each protein concentration (10, 20, 30, 40, and 50 nM) to determine the reproducibility of the signal and to control injections to assess the stability of the RNA surface during the experiment. Dissociation constants were calculated using the BIA Evaluation 3.0 software package, according to the fitting model 1:1 Languimir binding.

Modeling of RNase R and Rrp44 Protein Structures—Three-dimensional models for *E. coli* RNase R (RNR_ECOLI) and human exosome complex exonuclease Rrp44 (Rrp44_HUMAN) proteins were performed using standard homology modeling methods based on the multiple sequence alignment of the family members, as described in supplemental experimental procedures.

TABLE 1

Exoribonucleolytic activity and RNA binding affinity of wild-type and mutant enzymes

Exoribonucleolytic activity was assayed using a 35-nt poly(A) chain as substrate. Activity assays were performed as described under "Experimental Procedures." The dissociation constants (K_D) were determined by surface plasmon resonance using Biacore 2000 with a 25-nt RNA oligomer (5′-biotin-CCC GAC ACC AAC CAC UAA AAA AAA A-3′).

Proteins	Exoribonucleolytic activity	Relative activity	Dissociation constants-K_D	Relative K_D
	nM/min	%	*nM*	
WT	29.9 ± 3.6	100[a]	6.48 ± 0.4	1.0
D201N	<0.1	0.2	11.4 ± 0.7	1.8
D207N	3.7 ± 0.6	12	13.4 ± 1.7	2.1
D209N	≪0.1	<0.1	5.3 ± 0.3	0.8
D210N	<0.1	0.3	11.4 ± 0.9	1.8
Y253A	7.7 ± 1.9	26	35.0 ± 3.5	5.5
F358A	62.6 ± 3.3	209	9.9 ± 0.3	1.5
Y253A,F358A	3.7 ± 0.3	12	5.1 ± 0.1	0.8

[a] Exoribonucleolytic activity of the wild-type enzyme was taken as 100%. The determination of the enzyme exoribonucleolytic activity was carried out by measuring and quantifying the disappearance of the substrate.

MD Simulation of 2ix1 Structure; Modeling of Wild-type Enzyme and Y253A Mutant—To obtain a theoretical dynamic model of RNase enzyme, the previously published x-ray structure of RNase II D209N mutant complexed with a 10-nt poly(A) RNA (Protein Data Bank code 2IX1) (23) was subjected to 4 ns of molecular dynamics (MD)[4] simulation. Re-creation was performed using the PMEMD module and the parm99 parameter set in the AMBER 8 package (27, 28). Based on the resultant *in silico* structure of the mutant, models for wild-type enzyme as well as for Y253A mutant were also generated by substituting appropriate residues using standard homology modeling procedures. Both structures were then subjected to a second MD running to simulate the possible modifications in the protein arrangement and its relationship to the substrate RNA as a result of the introduced changes. Details on the MD method are described in supplemental experimental procedures.

Multiple Sequence Alignment—Homologous sequences belonging to the RNase II, RNase R, and Rrp44 family of proteins were obtained in protein data bases using BLAST (29) and were aligned using ClustalW (30) and T-COFFEE (31) algorithms.

RESULTS AND DISCUSSION

Mutations in the Aromatic Residues That Clamp the RNA Can Alter the End Products—To further determine the role of Tyr-253 and Phe-358 in RNA decay, we mutated these aromatic residues into an alanine and constructed single (Y253A or F358A) and double (Y253A,F358A) mutants. In RNase II the RNA molecule (nt 9–13) is stacked and clamped between the aromatic residues Tyr-253 and Phe-358. Based on structure, we would predict that RNase II would be inactive in the absence of Tyr-253, because the unclamping of the RNA at the active site would disrupt the correct conformation of the substrate, thus impairing catalysis. However, by changing Tyr-253 to Ala 26% of the activity of the enzyme persisted (Table 1 and Fig. 2). Dynamic models built from the crystallographic structure of the RNase II-RNA complex reveal that, in fact, Tyr-253 remains firmly stacked to the putative outgoing nt 13 by its respective aromatic system, even after 4 ns of molecular dynamics simulation and despite the *anti* to *syn* conformational change exhibited by the adenine nucleotide (Fig. 3*A* and supplemental Fig. S3). This result supports that Tyr-253 is actually important for the maintenance of the RNA clamping in RNase II. However, despite its conservation, there must be other residues and contacts at the catalytic cavity that are sufficient for the RNA to bind to the protein. In fact, Phe-250 and Phe-257 residues, located in close vicinity to Tyr-253, could presumably account for such a role, although the corresponding model would require a conformational reorganization of the protein backbone around these positions. Nevertheless, the most surprising result was that the Y253A mutant changed the smallest product of degradation of RNase II from 4 to 10 nt (Fig. 2), an end product not observed before. It is known that for a processive degradation by RNase II the RNA molecule must bind simultaneously to the anchoring and catalytic regions (14, 23). Moreover, the three-dimensional model of the RNase II-RNA complex revealed that a 10-nt fragment is the minimum length of the RNA molecule that is still able to contact both the anchoring and the catalytic regions (23). RNA molecules shorter than 10 nt only establish interactions with the catalytic region, and consequently degradation becomes distributive. In Y253A the absence of Tyr-253 may cause the loosening of the RNA substrate at the catalytic site and, as a consequence, the binding at the anchoring region is essential for the RNA to remain attached to the enzyme. For this reason, RNA is degraded up to 10 nt and the RNA fragment is then released from the enzyme, being therefore the smallest degradation product generated in the Y253A mutant. As such, Tyr-253 must play an essential role in the attachment of the 3′-end of the RNA substrate to the catalytic region. In agreement, the K_D value obtained for Y253A by surface plasmon resonance analysis is 5.5-fold higher than that of the wild-type enzyme (Table 1 and supplemental Fig. S4), and this shows that Y253A substitution significantly impaired RNA binding. Moreover, the modeled structures of Y253A show that, once the Tyr-253-nt 13 stacking is lost, the RNA suffers a large rearrangement, coordinated by corresponding counter movements of contacting RNase II catalytic domain structure (Fig. 3*A* and supplemental Fig. S3*B*). Surprisingly, these movements do not appear to affect directly the geometry of the Asp residues in the active center, thus explaining the remaining catalytic activity of the Y253A mutant.

When analyzing the F358A mutant we found that, unexpectedly, the protein was 2-fold more active than the wild-type (Table 1). Although the smallest degradation product detected was 4 nt, similar to the wild-type, there was a visible product of 5 nt (Fig. 2). This may suggest that Phe-358 is acting as a "propeller," helping to push the last 5 nt toward the catalytic site, until the final product is a 4-nt fragment. However, the K_D was not dramatically affected by this mutation because it was <2-fold higher than that of the wild-type enzyme, suggesting that Phe-358 may be playing a more accessory role in the maintenance of the proper RNA conformation. This hypothesis was confirmed by MD of the structure, which contrary to the data revealed by the three-dimensional structure suggests that the dynamic stability of the Phe-358 stacking could be compromised in the simulation conditions in the general AMBER force

[4] The abbreviation used is: MD, molecular dynamics.

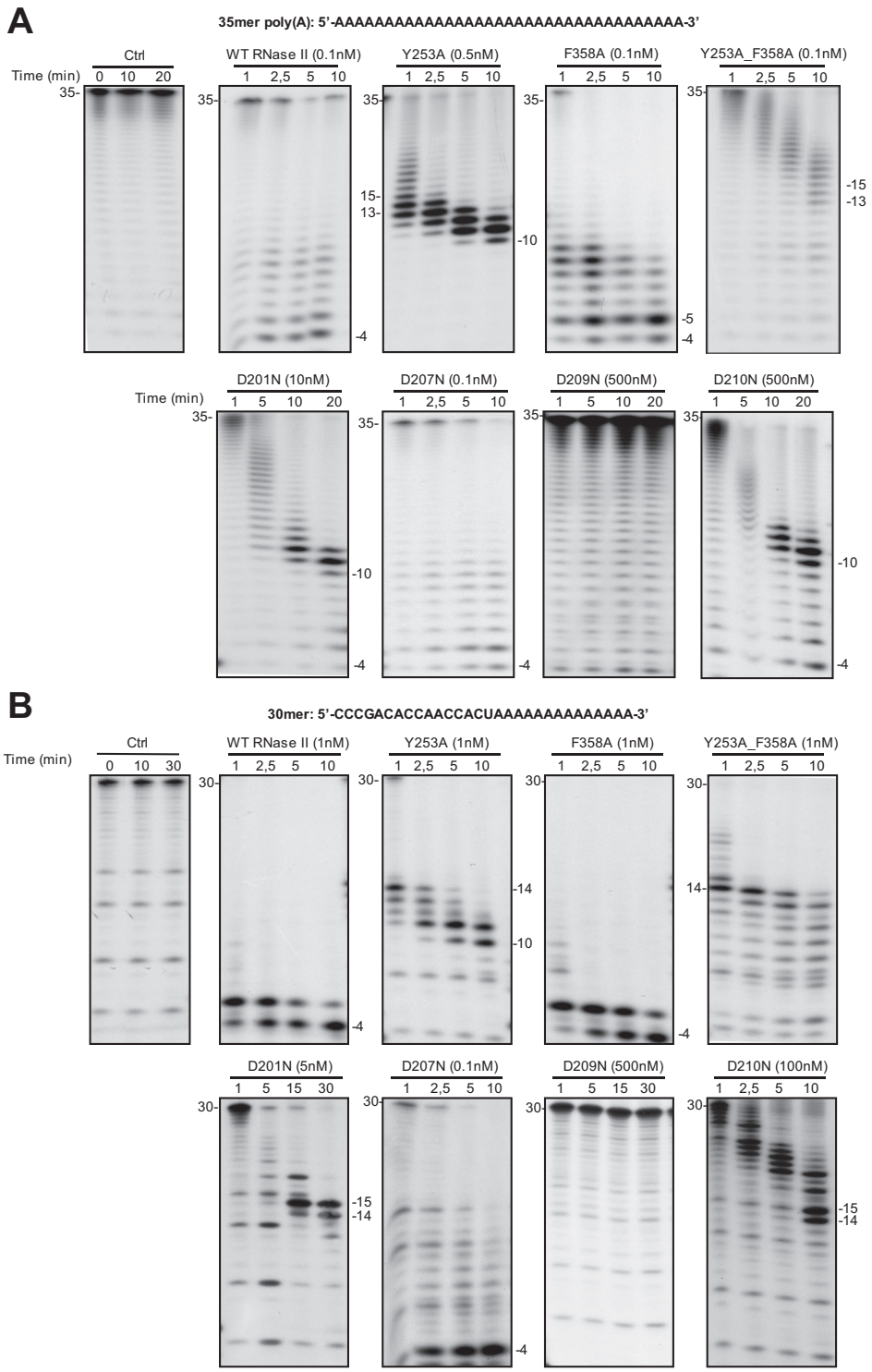

FIGURE 2. **Exoribonuclease activity: comparison of wild-type and mutants.** Activity assays were performed as described under "Experimental Procedures" using a poly(A) chain of 35 nt (*A*) or a 30-mer oligoribonucleotide (*B*) as substrate. The mutants used and their respective protein concentrations are shown. The wild-type enzyme was used as control. Samples were taken during the reaction at the time points indicated, and reaction products were analyzed in a 20% polyacrylamide/7 M urea gel. Control reactions with no enzyme added (*Ctrl*) were incubated at the maximum reaction time for each protein. Length of substrates and degradation products are indicated.

field (27, 28). Nevertheless, in accordance with the experimental results obtained for the F358A mutant, a less active structural role of this residue during catalysis could still be compatible with the real structural data. Therefore, Phe-358 is not equivalent in function to Tyr-253 and, unlike the latter, Phe-358 is not present in all members of the RNase II family (supplemental Fig. S5). Computational models also support that the structural role of these residues in RNA stabilization could also be quite different. Tyr-253 would be responsible for the stacking-mediated stabilization of the outgoing nucleotide at the 3′-end during catalysis (Fig. 3*A*), while the partially conserved Phe-358 position could mediate the transition of the RNA by providing the appropriate hydrophobic environment to prevent spurious contacts. In turn, substitution by a smaller hydrophobic residue, such as alanine, could modify the RNA stability in that region, thus biasing the rate of processing.

The double mutant Y253A,F358A behaved similar to Y253A regarding the size of the smallest product generated, because the end product obtained was 13–15 nt (Fig. 2). However, we detected a decrease in activity (12 *versus* 26%) although the RNA binding affinity was not significantly affected ($K_D = 5.1 \pm 0.1$ nM) (Table 1). Therefore, it seems that the F358A mutation may somehow compensate the absence of Tyr-253 in RNA binding, perhaps allowing an alternative accommodation of the RNA in the catalytic cavity.

To compare RNase II with other family members, we constructed the structural models of *E. coli* RNase R and human Rrp44 proteins based on the RNase II structure (Fig. 1, *B* and *C*). The results clearly indicate that these three enzymes share a common three-dimensional arrangement, being all the critical residues for exoribonucleolytic activity located in equivalent spatial positions. Comparing the three protein models (Fig. 1), it is noteworthy that they have a common arrangement of the clamping tyrosine amino acid. In contrast, the presence of Phe-358 is exclusive to RNase II (supplemental Fig. S5). RNase R protein presents a Phe residue in the immediate downstream position (Phe-429 in RNR_ECOLI sequence), perhaps with a similar functionality in RNA fixing. However, an equivalent residue is completely absent in Rrp44 sequences, where it is substituted mainly by polar residues with uncharged R-groups (Asn and Thr) (supple-

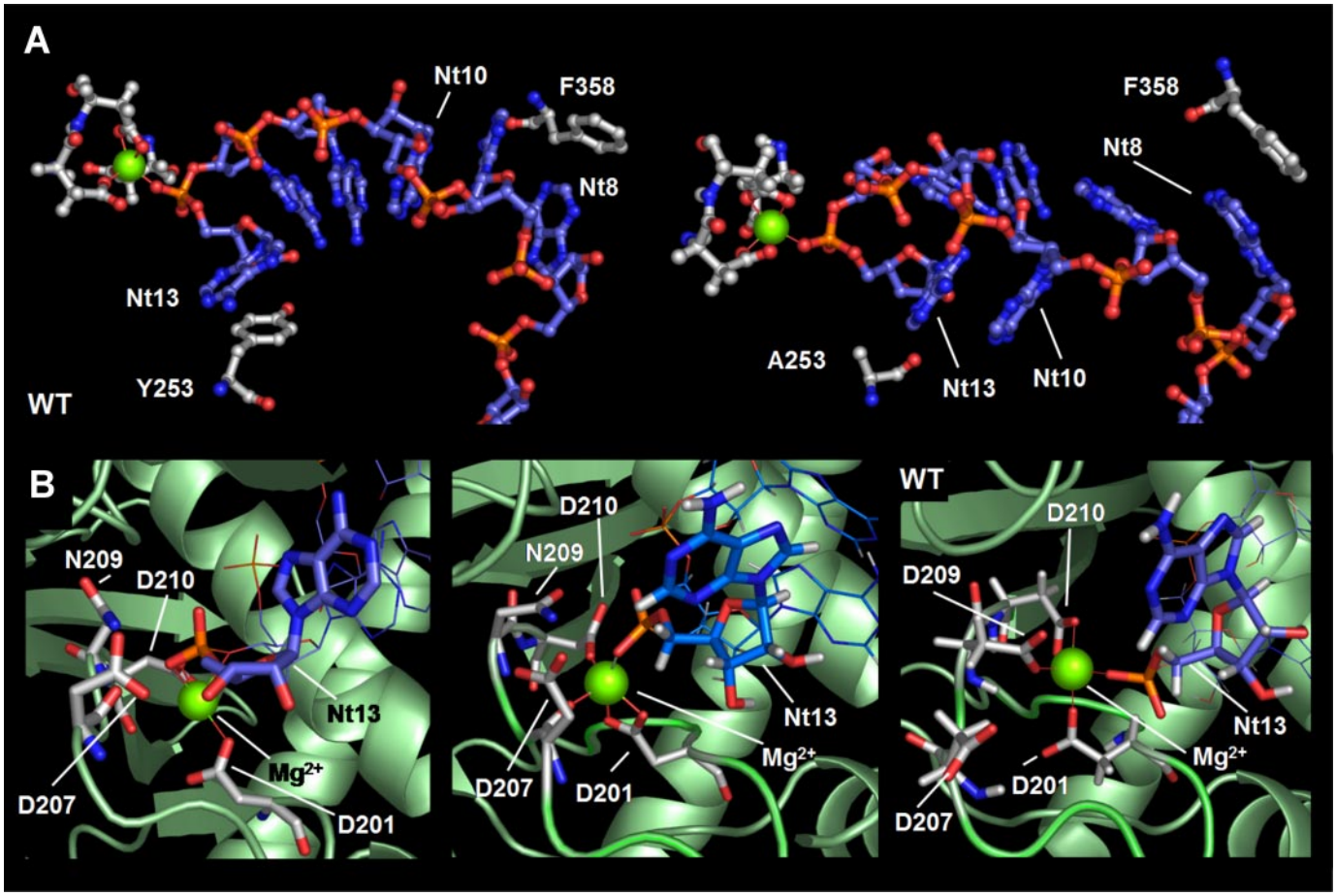

FIGURE 3. **Modeling active center and RNA binding in wild-type and mutant RNase II proteins.** Crystal structure 2ix1 (RNase II-Asp-209 mutant complexed with the RNA) was subjected to molecular dynamics equilibration for 4 ns. The wild-type enzyme and Y253A mutant were modeled and subjected again to equilibration for 1 ns. *A*, relative position of the RNA molecule in wild-type (*left*) and Y253A mutant (*right*) enzymes after 1 ns of molecular dynamics. Despite the lack of notable differences in Asp residues surrounding the Mg^{2+} ion in the active center, the Y253A mutation results in large reorganization of RNA, implicating differences in base-stacking among nucleotides themselves as well as between them and Tyr-253 and Phe-358 residues, probably resulting in loss of stability for RNA positioning. *B*, residues surrounding the active center of the enzyme. *Left*, initial 2ix1 -D209N- crystal structure. *Center*, model for the D209N mutant after 4 ns of MD, showing that whereas Asn-209 does not contact with the Mg^{2+} ion, Asp-207 coordinates it through its backbone CO group. *Right*, MD model for wild-type RNase II showing Asp-209, but not Asp-207, contacting Mg^{2+} in addition to Asp-201, Asp-210, and the phosphate group of nt 13.

mental Fig. S5). The differences in the equivalent amino acid Phe-358 in RNase II, RNase R, and Rrp44 enzymes could explain their differences in regard to RNA degradation. For instance, the final end product of both RNase II and Rrp44 is 4 nt, whereas for RNase R it is a 2-nt fragment (2, 13, 15, 23).

The Highly Conserved Aspartates in RNase II Active Site Are Not Equivalent in Their Role in Catalysis—Four highly conserved aspartic acids, Asp-201, Asp-207, Asp-209, and Asp-210, are located in the RNase II active site. It has been postulated that their function is to position the RNA substrate correctly and promote the nucleophilic attack of the phosphodiester bond (23, 32). The single substitution of Asp-209 by Asn in RNase II (D209N) has been shown to be responsible for the total loss of RNase II activity without affecting RNA binding ability (32) (Table 1 and Fig. 2). A similar mutation in the yeast RNase II homologue Dis3/Rrp44 (D551N) totally abolished activity without reducing substrate binding and was responsible for a very strong growth defect, suggesting that the phenotype of this mutant is very important for yeast physiology (19, 20).

To understand the precise role of these residues, we mutated residues Asp-201, Asp-207, and Asp-210 to asparagines. Our results revealed that mutations in both Asp-201 and Asp-210 lead to a significant loss of activity in degradation of poly(A) (0.2 and 0.3% of that of the wild-type enzyme, respectively) (Table 1). Aspartates 201 and 210 were proposed to be coordinating the Mg^{2+} ion that is essential for catalysis together with two water molecules and two oxygen atoms of the RNA substrate (23). The substitution of these aspartates by asparagines would result in the loss of one of the coordinations, thus destabilizing the cation at the active site and impairing the reaction. Similar reduction in activity was observed with the 30 single-stranded substrate (Fig. 2*B*). Both D201N and D210N mutants generated a 10–11-nt fragment as a major degradation product, although longer reaction times resulted in the usual 4-nt fragment as a secondary product (Fig. 2*A*). The absence of these aspartates may destabilize the attachment of the RNA at the catalytic site, because both residues are contributing to the binding of the RNA at this region, either directly (by Asp-201) or through the Mg^{2+} ion they chelate (Asp-201 and Asp-210) (23). As such, fragments below 10 nt in length, when the binding of the substrate to the anchor region is no longer possible, lead to a distributive degradation, explaining this destabilization. Interestingly, the degradation of the 30 single-stranded seems to stop

after digestion of 15–16 nt, thus generating a 14–15-nt fragment as a final product (Fig. 2*B*). This substrate contains a 16-nt poly(A) tail at its 3′-end, and both D201N and D210N mutant enzymes degrade this tail to completion and then stop. This effect reflects a marked preference by poly(A) substrate that has also been observed in the wild-type enzyme (13–15) but seems to be more pronounced in these two mutants.

The role of Asp-207 does not seem to be so critical for catalysis when compared with the other mutants because after its substitution by asparagine the enzyme still retains 12% activity (Table 1 and Fig. 2). This result differs from previously published data in which the mutation of Asp-207 to alanine led to a more significant loss of activity (2.5% of that of the wild-type enzyme) (25). However, the substitution of an aspartate by alanine may cause local conformational changes other than those generated by the substitution by asparagine in which only the acidic nature of the residue is altered. The structure of the RNase II D209N mutant revealed that Asp-207 is within H-bonding distance of the 3′-OH group of the RNA molecule (Fig. 3*B*). In contrast, after molecular dynamics equilibration during 4 ns, this close contact apparently disappeared and Asp-207 was then positioned in contact with the Mg^{2+} ion in the active center via its backbone CO group (Fig. 3*B*). Surprisingly, when the wild-type protein was modeled and subjected again to molecular dynamics processes, Asp-209 was located in contact with the Mg^{2+} atom, in the active center, resulting in the displacement of Asp-207 to a far position (Fig. 3*B*). As a result of this analysis, Asp-207 does not appear to play such a critical role. Perhaps it only contributes to the general maintenance of the appropriate position of both water and ions, which explains in part the remaining activity of D207N.

As expected, D209N was totally inactive in the degradation of the two substrates tested (Table 1 and Fig. 2), reinforcing the key role of Asp-209 in catalysis. In the three mutant proteins D201N, D207N, and D210N, the K_D ranged between 11 and 14 nM, only 2-fold higher than the wild-type RNase II enzyme (Table 1), thus showing only a slight reduction in the RNA binding affinity. Therefore it seems that aspartates 201, 207, and 210 are not directly involved in the RNA binding (Table 1). In fact, in the crystal structure these three residues interact with the RNA substrate at the active site via the Mg^{2+} ion or by being directly bound to the leaving nucleotide (23). Disruption of such interactions by these mutations would cause the loosening of the RNA at the active site.

Moreover, the three-dimensional models of *E. coli* RNase R and human Rrp44 proteins (Fig. 1, *B* and *C*) revealed that these four aspartic residues have spatial positions equivalent to those in RNase II. Therefore, we can propose similar catalytic roles for these residues in these two RNase II-like enzymes.

In this report we have improved the proposed model for RNA degradation by RNase II by defining the precise role and function of some highly conserved residues present in the active site of the enzyme. We conclude that Tyr-253 and Phe-358 are not essential for catalysis by RNase II, because the enzyme still retains activity after the substitution of these residues by alanines. However, Tyr-253 seems to be a critical residue in setting the smallest product generated by RNase II under the conditions tested. This accentuates the importance of this residue in the stabilization of the 3′-end of the RNA molecule. Tyr-253 is highly conserved and equivalent residues are present in many RNase II family members (supplemental Fig. S5). Taking into account the functional and structural similarities to Rrp44 (20), these conclusions will be particularly important for the evaluation of the role of this residue in recognition, binding, and degradation of different RNA targets. The substitution of Phe-358 results in the increase by 2-fold of the activity of the enzyme. This result suggests that Phe-358 could be preventing a faster degradation of the RNA by stalling its translocation, probably due to the stacking of its aromatic ring between the bases of contiguous nucleotides. Furthermore, we show that the highly conserved aspartates Asp-201, Asp-207, Asp-209, and Asp-210 are not equivalent and that their functions in RNA metabolism are distinct, with Asp-209 being the only residue essential for RNase II activity.

Moreover, the structural models of *E. coli* RNase R and human Rrp44 proteins showed an overall structure similar to that of the RNase II, with the critical residues in similar spatial positions. In addition, the structure of yeast Rrp44 showed that *E. coli* RNase II is a good model and suggests that the RNA recruitment mechanism is conserved. As such, we can hypothesize and extrapolate our findings to related members of the RNase II family.

This study sheds new light on the model previously proposed for RNA degradation by RNase II. In addition, the fact that the RNase II homologue is the only catalytically active nuclease in the exosome highlights the need to unravel the precise role of highly conserved residues. Finally, these results can be applied to better understand the decay mechanisms for all RNase II family members that have revealed a similar mode of action, including those present in the exosome.

Acknowledgments—We thank Ambro Van-Hoof for critical reading and Gonçalo da Costa for advice on the plasmon resonance analysis (Biacore). We also thank Jesús Mendieta for helpful discussions in molecular dynamics approaches and Biomol-Informatics SL for bioinformatics consulting.

REFERENCES

1. Mian, I. S. (1997) *Nucleic Acids Res.* **25,** 3187–3195
2. Mitchell, P., Petfalski, E., Shevchenko, A., Mann, M., and Tollervey, D. (1997) *Cell* **91,** 457–466
3. Grossman, D., and van Hoof, A. (2006) *Nat. Struct. Mol. Biol.* **13,** 760–761
4. Zuo, Y., and Deutscher, M. P. (2001) *Nucleic Acids Res.* **209,** 1017–1026
5. Cairrão, F., Chora, A., Zilhão, R., Carpousis, J., and Arraiano, C. M. (2001) *Mol. Microbiol.* **276,** 19172–19181
6. Andrade, J. M., Cairrão, F., and Arraiano, C. M. (2006) *Mol. Microbiol.* **60,** 219–228
7. Cairrão, F., Arraiano, C., and Newbury, S. (2005) *Dev. Dyn.* **232,** 733–737
8. Zilhão, R., Cairrão, F., Régnier, P., and Arraiano, C. M. (1996) *Mol. Microbiol.* **20,** 1033–1042
9. Zilhão, R., Regnier, P., and Arraiano, C. M. (1995) *FEMS Microbiol. Lett.* **130,** 237–244
10. Cairrão, F., and Arraiano, C. M. (2006) *Biochem. Biophys. Res. Commun.* **343,** 731–737
11. Bollenbach, T. J., Lange, H., Gutierrez, R., Erhardt, M., Stern, D. B., and Gagliardi, D. (2005) *Nucleic Acids Res.* **33,** 2751–2763
12. Lim, J., Kuroki, T., Ozaki, K., Kohsaki, H., Yamori, T., Tsuruo, T., Nakamori, S., Imaoka, S., Endo, M., and Nakamura, Y. (1997) *Cancer*

Res. **57,** 921–925
13. Amblar, M., Barbas, A., Fialho, A. M., and Arraiano, C. M. (2006) *J. Mol. Biol.* **360,** 921–933
14. Cannistraro, V. J., and Kennell, D. (1994) *J. Mol. Biol.* **243,** 930–943
15. Amblar, M., Barbas, A., Gomez-Puertas, P., and Arraiano, C. M. (2007) *RNA* (*N.Y.*) **13,** 317–327
16. Orban, T. I., and Izaurralde, E. (2005) *RNA* (*N.Y.*) **11,** 459–469
17. Lejeune, F., Li, X., and Maquat, L. E. (2003) *Mol. Cell* **12,** 675–687
18. LaCava, J., Houseley, J., Saveanu, C., Petfalski, E., Thompson, E., Jacquier, A., and Tollervey, D. (2005) *Cell* **121,** 713–724
19. Dziembowski, A., Lorentzen, E., Conti, E., and Seraphin, B. (2007) *Nat. Struct. Mol. Biol.* **14,** 15–22
20. Schneider, C., Anderson, J. T., and Tollervey, D. (2007) *Mol. Cell* **27,** 324–331
21. Liu, Q., Greimann, J. C., and Lima, C. D. (2006) *Cell* **127,** 1223–1237
22. Wang, H. W., Wang, J., Ding, F., Callahan, K., Bratkowski, J., Butler, J. S., Nogles, E., and Ke, A. (2007) *Proc. Natl. Acad. Sci. U. S. A.* **104,** 16844–16849
23. Frazão, C., McVey, C. E., Amblar, M., Barbas, A., Vonrhein, C., Arraiano, C. M., and Carrondo, M. A. (2006) *Nature* **443,** 110–114
24. McVey, C. E., Amblar, M., Barbas, A., Cairrão, F., Coelho, R., Romão, C., Arraiano, C. M., Carrondo, M. A., and Frazão, C. (2006) *Acta Crystallogr. Sect. F* **62,** 684–687
25. Zuo, Y., Vincent, H. A., Zhang, J., Wang, Y., Deutscher, M. P., and Malhotra, A. (2006) *Mol. Cell* **24,** 149–156
26. Higuchi, R. (1990) in *PCR Protocols, A Guide to Methods and Applications* (Innis, M. A., Gelfand, D. H., Sninsky, J. J., and White, T. J., eds) pp. 177–183 Academic Press, Inc./Harcourt Brace Jovanovich, San Diego, CA
27. Case, D. A., Cheatham, T. E., III, Darden, T., Gohlke, H., Luo, R., Merz, K. M., Jr., Onufriev, A., Simmerling, C., Wang, B., and Woods, R. J. (2005) *J. Comput. Chem.* **26,** 1668–1688
28. Case, D. A., Darden, T., Cheatham, T. E., III, Simmerling, C., Wang, J., Duke, R. E., Luo, R., Merz, K. M., Jr., Wang, B., Pearlman, D. A., Crowley, M., Brozell, S., Tsui, V., Gohlke, H., Mongan, J., Hornak, V., Cui, G., Beroza, P., Schafmeister, C., Caldwell, J. W., Ross, W. S., and Kollman, P. A. (2004) *AMBER 8*, University of California, San Francisco
29. Altschul, S. F., Madden, T. L., Schaffer, A. A., Zhang, J., Zhang, Z., Miller, W., and Lipman, D. J. (1997) *Nucleic Acids Res.* **25,** 3389–3402
30. Thompson, J. D., Higgins, D. G., and Gibson, T. J. (1994) *Nucleic Acids Res.* **22,** 4673–4680
31. Notredame, C., Higgins, D. G., and Heringa, J. (2000) *J. Mol. Biol.* **302,** 205–217
32. Amblar, M., and Arraiano, C. M. (2005) *FEBS J.* **272,** 363–374